Demonstration of 4.3 Pbps Optical Circuit Switching for Intra-Datacentre Networks Based on Spatial Super-Channels

Eiji Honda[(1)], Yojiro Mori[(1)], Hiroshi Hasegawa[(1)], Ken-ichi Sato[(2)]

[(1)] Nagoya University, e_honda@nuee.nagoya-u.ac.jp
[(2)] National Institute of Advanced Industrial Science and Technology (AIST)

Abstract *We verify the feasibility of the optical circuit switch architecture for intra-datacentre networks based on spatial super-channels using DP-QPSK, DP-8QAM, and DP-16QAM signals. Simulations clarify the maximum throughput attainable with each modulation format. Experiments demonstrate a switch throughput of 4.3 Pbps.*

Introduction

Intra-datacentre traffic is exploding due to the spread of cloud-computing services and video-streaming services. The total amount of intra-datacentre traffic is about five times that of IP traffic. In order to process the large amounts of intra-datacentre traffic cost-effectively, optical switch networks and opto-electronic hybrid switch networks have been proposed[1]–[5]. In both switch networks, the high-throughput and high-port-count optical circuit switch plays a key role to transmit signals without using costly optical-electrical-optical conversion. In order to realize such switching systems, many types of optical circuit switch architectures are being intensively studied[6]–[16]. We have proposed an optical circuit switch architecture that combines delivery-and-coupling (DC) planar space switches and wavelength-routing (WR) switches[16]. With this architecture, we demonstrated 153.6 Tbps throughput with a 1536×1536 optical circuit switch[17].

To further expand the total switch throughput, we introduced spatial super-channels to our switch architecture[18]. The proposed scheme can increase the throughput without increasing the switch hardware cost per bit. We demonstrated the switch throughput of 2.1 Pbps[18].

In this paper, we investigate in detail the parameter dependency of the optical switch architecture based on spatial super-channels. Simulations and experiments demonstrate the switch throughput of 4.3 Pbps with DP-QPSK signals, 3.2 Pbps with DP-8QAM signals, and 2.1 Pbps with DP-16QAM signals.

Switching network architecture based on spatial super-channels

Figure 1 depicts the switch architecture based on spatial super-channels[18]. The switch comprises *MN* wavelength-tuneable transmitters, *LN* *M*×*M* DC planar space switches, *LM* *N*×*N* WR switches, and *MN* receivers, where *M* stands for the port count of the DC switch, and *N* is the number of wavelengths. Each pair of transmitter and receiver supports *L* spatial sub-channels and *N* wavelengths. An *M*×*M* DC switch consists of *M* 1×*M* optical selectors and *M* *M*×1 optical couplers. An *N*×*N* WR switch is composed of *n* (*N*/*n*)×1 optical couplers, *n* erbium-doped fibre amplifiers (EDFAs), and an *n*×*N* uniform-loss and cyclic-frequency (ULCF) AWG[17]. An *n*×*N* ULCF AWG decreases the degree of couplers needed for signal aggregation by *n* compared with a 1×*N* AWG, i.e., the loss of the WR switch is reduced.

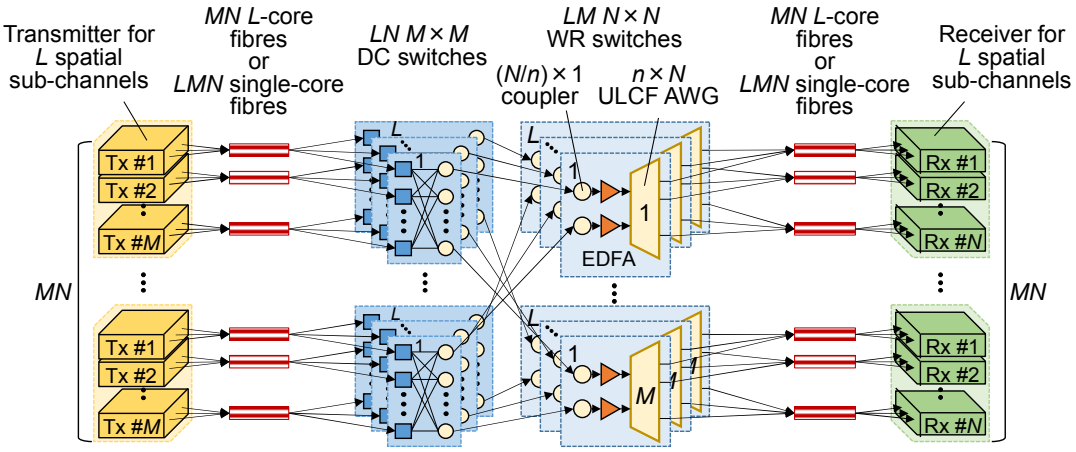

Fig. 1: Switch architecture based on spatial super-channels (An *M*×*M* DC switch consists of 1×*M* selectors and *M*×1 couplers)

The switching operation is as follows: A transmitter outputs L sub-channel signals, where the wavelength is selected according to the combination of the input port number and target output port number of the ULCF AWG. L sub-channels are input to the DC-switch part via a spatially multiplexed transmission link, e.g. an L-core fibre and L single-core fibres. In the DC-switch part, the L sub-channels are jointly directed to a WR-switch part. Here, the M×1 coupler in the DC switch combines the signals from the input ports. In the WR-switch part, multiple wavelength signals are aggregated by an (N/n)×1 optical coupler. After amplification, the signals are divided according to wavelength by an n×N ULCF AWG. Finally, the target receiver detects the L sub-channels output from the ULCF AWG.

Simulations

We conduct computer simulations to evaluate the attainable port count and throughput of the switch. As the sub-channel signal, we use 32-Gbaud 100-Gbps DP-QPSK signals, 150-Gbps DP-8QAM signals, and 200-Gbps DP-16QAM signals. We assume 96 wavelengths aligned on the 50 GHz grid in the C-band. Each channel has 7 spatial sub-channels. Transmitter output power of a sub-channel is parameterised. Other specifications of the simulation are as shown below: The loss of the spatially multiplexed transmission link is 3.5 dB. The losses of the 1×M selector and M×1 coupler in an M×M DC switch are set to ceil($\log_2 M$)×0.5 dB and ceil($\log_2 M$)×3.5 dB, respectively. Here, M-1 signals from the other input ports of the DC switch are input to the coupler as intra-band crosstalk; the extinction ratio of the DC switch is set to 35 dB. The degree of a signal aggregation coupler in the WR-switch part, N/n, is 8; the loss of the coupler is set to 10.5 dB. To alleviate the signal degradation yielded by frequency deviation of the AWG passbands, we use 12 1×2 splitters and a pair of interleaved 12×48 ULCF AWGs instead of a single 12×96 ULCF AWG[17]. The losses of the 1×2 splitter and the 12×48 ULCF AWG are set to 3.5 dB and 9 dB, respectively. The noise figure and saturation power of the EDFA are 5 dB and 20 dBm, respectively. Here, intra-band crosstalk signals are input to the remaining 11 input ports of the ULCF AWG; the extinction ratio is set to 32 dB. The allowable maximum bit-error ratio (BER) is set to 10^{-2} assuming the use of forward-error correction.

Figure 2 shows the relationships between the maximum switch port count and transmitter power using each modulation format. For instance, when the transmitter power is 0 dBm, a 6144×6144 switch is attainable with 100-Gbps DP-QPSK signals, a 3072×3072 switch is attainable with 150-Gbps DP-8QAM signals, and a 1536×1536 switch is attainable with 200-Gbps DP-16QAM signals. Figure 3 shows maximum switch throughputs for each modulation format. When the transmitter power is the same, 100-Gbps DP-QPSK signals offer the best performance in terms of total throughput. However, the hardware cost is highest due to the

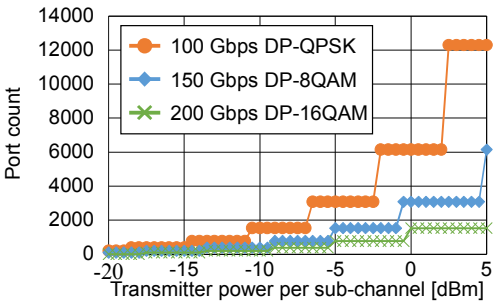

Fig. 2: Maximum switch port counts for each modulation format versus transmitter power

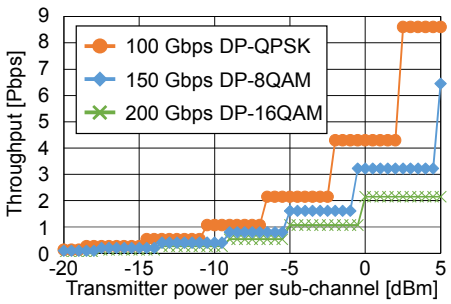

Fig. 3: Maximum switch throughputs for each modulation format versus transmitter power

Tab. 1: The numbers of switch components required to construct the switch with throughput of $LMNB$ (sub-channel bitrates of QPSK, 8QAM, and 16QAM are B, 3B/2, and 2B, respectively)

	QPSK		8QAM		16QAM	
	-	Compared with QPSK	-	Compared with QPSK	-	Compared with QPSK
Number of transmitters/receivers	MN	1	2MN/3	**2/3**	MN/2	**1/2**
Number of DC switches	LN	1	LN	1	LN	1
Port count of a DC switch	M	1	2M/3	**2/3**	M/2	**1/2**
Number of WR switches	LM	1	2LM/3	**2/3**	LM/2	**1/2**
Number of EDFAs	nLM	1	2nLM/3	**2/3**	nLM/2	**1/2**
Number of AWGs	LM	1	2LM/3	**2/3**	LM/2	**1/2**

lowest spectral efficiency. Table 1 summarises the required numbers of switch components needed with each modulation format. Since the required numbers of costly transmitter lasers and EDFAs are reduced, using higher-order modulation formats can construct switches with lower cost. For example, using 200-Gbps DP-16QAM signals can halve the numbers of transmitters and EDFAs compared with using 100-Gbps DP-QPSK signals with the same switch throughput. Thus, the modulation order should be selected considering the target port count and throughput.

Experiments

To confirm the switch performance, we conducted experiments. Figure 4 shows the experimental setup. According to the simulation results, we constructed part of 6144×6144 optical circuit switch for QPSK signals with DC-switch scale *M* of 64, part of 3072×3072 switch for 8QAM signals with DC-switch scale *M* of 32, and part of 1536×1536 switch for 16QAM signals with DC-switch scale *M* of 16. Transmitter output powers were determined according to the simulation results with additional 2 dB margin; the output powers for QPSK, 8QAM, and 16QAM signals are 0 dBm, 1.5 dBm, and 2 dBm, respectively. The number of wavelengths is 96 in the full C-band. The transponders and switch ports were connected by 1-km 7-core fibres. We measured BERs of all combinations of 96 wavelengths and 7 spatial sub-channels for each modulation format.

Figures 5(a), (b), and (c) plot the measured BERs of 100-Gbps DP-QPSK signals, 150-Gbps DP-8QAM signals, and 200-Gbps DP-16QAM signals, respectively. We confirmed that all BERs achieved the target value of 10^{-2}. The overall throughputs are 4.3 Pbps (=6144×7×100 Gbps), 3.2 Pbps (=3072×7×150 Gbps), and 2.1 Pbps (=1536×7×200 Gbps) when QPSK, 8QAM, and 16QAM signals are used, respectively.

Conclusions

We verified the feasibility of the switch architecture based on spatial super-channels with various design parameter values. We conducted simulations and experiments on 100-Gbps DP-QPSK, 150-Gbps DP-8QAM and 200-Gbps DP-16QAM signals. The switch throughput of 4.3 Pbps was experimentally demonstrated by passing 7×100-Gbps DP-QPSK signals across part of a 6144×6144 optical switch.

Acknowledgements

This paper is based on results obtained from a project JPNP16007 commissioned by the New Energy and Industrial Technology Development Organization (NEDO). This work was also supported by KAKENHI (18K13756).

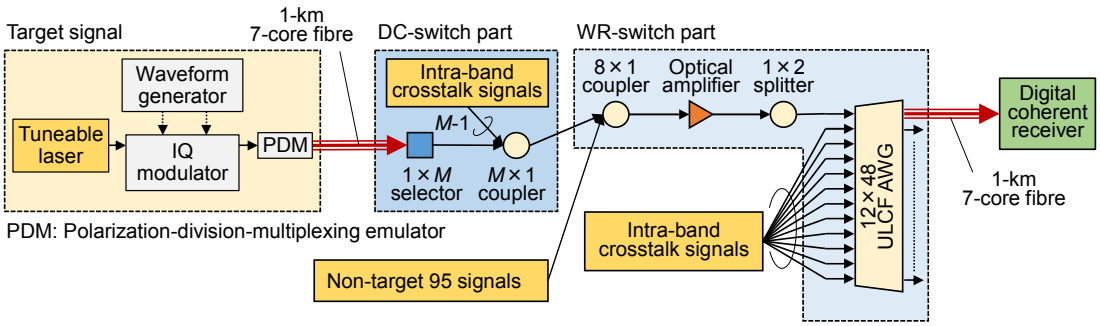

Fig. 4: Experimental setup

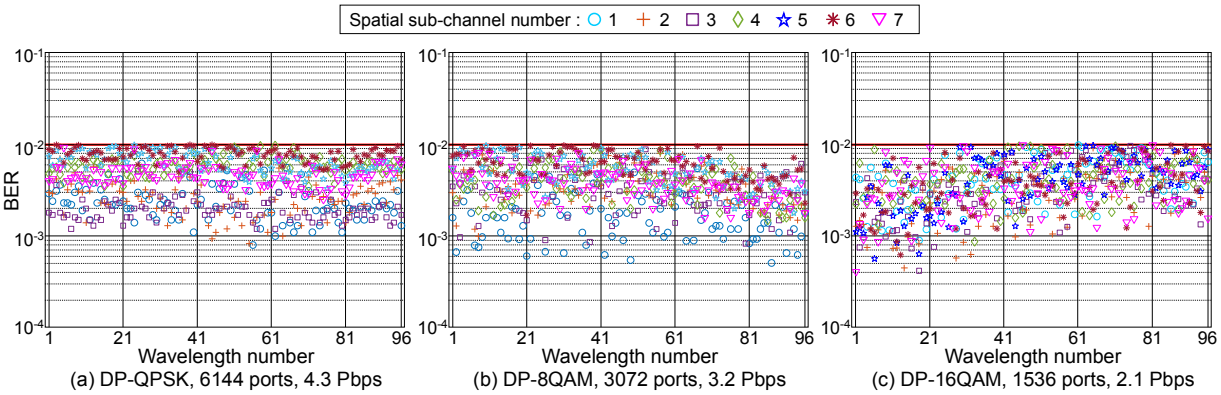

Fig. 5: BERs measured on all combinations of 96 wavelengths and 7 spatial sub-channels for each modulation format

References

[1] N. Farrington *et al.*, “Helios: a hybrid electrical/optical switch architecture for modular data centers”, in *Proc. ACM SIGCOMM 2010 Conference (SIGCOMM '10)*, New Delhi, India, Aug. 2010, pp. 339–350.

[2] C. Kachris and I. Tomkos, “A survey on optical interconnects for data centers”, *IEEE Commun. Surv. Tutorials*, vol. 14, pp. 1021–1036, Jan. 2012.

[3] W. M. Mellette *et al.*, “RotorNet: A Scalable, Low-complexity, Optical Datacenter Network”, in *Proc. ACM SIGCOMM 2017 Conference (SIGCOMM '17)*, Los Angeles, USA, Aug. 2017, pp. 267–280.

[4] F. Yan, X. Xue, and N. Calabretta, “HiFOST: a scalable and low-latency hybrid data center network architecture based on flow-controlled fast optical switches”, *IEEE/OSA J. Opt. Commun. Netw.*, vol. 10, pp. 1–14, July 2018.

[5] X. Xue *et al.*, “Experimental assessments of a flexible optical data center network based on integrated wavelength selective switch”, in *Proc. Optical Fiber Communication Conference (OFC)*, San Diego, USA, Mar. 2020, W1F.5.

[6] Q. Cheng *et al.*, “Demonstration of the feasibility of large-port-count optical switching using a hybrid Mach–Zehnder interferometer–semiconductor optical amplifier switch module in a recirculating loop”, *OSA Opt. Lett.*, vol. 39, pp. 5244–5247, Dec. 2014.

[7] W. M. Mellette *et al.*, “A Scalable, Partially Configurable Optical Switch for Data Center Networks”, *IEEE/OSA J. Lightw. Technol.*, vol. 35, pp. 136–144, Dec. 2016.

[8] A. C. Funnell *et al.*, “Hybrid Wavelength Switched-TDMA High Port Count All-Optical Data Centre Switch”, *IEEE/OSA J. Lightw. Technol.*, vol. 35, pp. 4438–4444, Aug. 2017.

[9] M. Ding *et al.*, “Hybrid MZI-SOA InGaAs/InP photonic integrated switches”, *IEEE J. Sel. Top. Quantum Electron.*, vol. 24, pp. 1–8, Oct. 2017.

[10] N. Terzenidis *et al.*, “High-port low-latency optical switch architecture with optical feed-forward buffering for 256-node disaggregated data centers”, *OSA Opt. Express*, vol. 26, pp. 8756–8766, Apr. 2018.

[11] R. Proietti *et al.*, “Experimental demonstration of a 64-port wavelength routing thin-CLOS system for data center switching architectures”, *IEEE/OSA J. Opt. Commun. Netw.*, vol. 10, pp. B49–B57, July 2018.

[12] K. Suzuki *et al.*, “Low-insertion-loss and power-efficient 32 × 32 silicon photonics switch with extremely high-Δ silica PLC connector”, *IEEE/OSA J. Lightw. Technol.*, vol. 37, pp. 116–122, Aug. 2018.

[13] Q. Cheng *et al.*, ”Ultralow-crosstalk, strictly non-blocking microring-based optical switch”, *OSA Photonics Res.*, vol. 7, pp. 155–161, Jan. 2019.

[14] T. J. Seok *et al.*, ” Wafer-scale silicon photonic switches beyond die size limit”, *OSA Optica*, vol. 6, pp. 490–494, Apr. 2019.

[15] K. Tanizawa *et al.*, “Optical time-slot switching with 5-μs guard time using 32×32 Si TO PILOSS switch”, in *Proc. 45th European Conference on Optical Communication (ECOC 2019)*, Dublin, Ireland, Sept. 2019, Th.1.A.

[16] K. Sato, “Realization and application of large-scale fast optical circuit switch for data center networking”, *IEEE/OSA J. Lightw. Technol.*, vol. 36, pp. 1411–1419, Feb. 2018.

[17] H. Nagai, Y. Mori, H. Hiroshi, and K. Sato, “Design and verification of large-scale optical circuit switch using ULCF AWGs for datacenter application”, *IEEE/OSA J. Opt. Commun. Netw.,* vol. 10, pp. 82–89, July 2018.

[18] E. Honda, Y. Mori, H. Hasegawa, and K. Sato, “High-throughput optical circuit switch for intra-datacenter networks based on spatial super-channels”, in *Proc. Optical Fiber Communication Conference (OFC)*, San Diego, USA, Mar. 2020, W1F.2.